Polymer 51 (2010) 1191–1196

Contents lists available at ScienceDirect

Polymer

journal homepage: www.elsevier.com/locate/polymer

# Electrically conductive polyethylene terephthalate/graphene nanocomposites prepared by melt compounding

Hao-Bin Zhang [a], Wen-Ge Zheng [a,*], Qing Yan [a], Yong Yang [a], Ji-Wen Wang [a], Zhao-Hui Lu [a], Guo-Ying Ji [a], Zhong-Zhen Yu [b,**]

[a] Ningbo Key Laboratory of Polymer Materials, Division of Polymers and Composites, Ningbo Institute of Material Technology & Engineering, Chinese Academy of Sciences, Ningbo 315201, China

[b] Beijing Key Laboratory on Preparation and Processing of Novel Polymeric Materials, Department of Polymer Engineering, College of Materials Science and Engineering, Beijing University of Chemical Technology, Beijing 100029, China

ARTICLE INFO

*Article history:*
Received 25 April 2009
Received in revised form
6 January 2010
Accepted 10 January 2010
Available online 18 January 2010

*Keywords:*
Graphene
Electrical conductivity
Melt compounding

ABSTRACT

Graphene nanosheets were prepared by complete oxidation of pristine graphite followed by thermal exfoliation and reduction. Polyethylene terephthalate (PET)/graphene nanocomposites were prepared by melt compounding. Transmission electron microscopy observation indicated that graphene nanosheets exhibited a uniform dispersion in PET matrix. The incorporation of graphene greatly improved the electrical conductivity of PET, resulting in a sharp transition from electrical insulator to semiconductor with a low percolation threshold of 0.47 vol.%. A high electrical conductivity of 2.11 S/m was achieved with only 3.0 vol.% of graphene. The low percolation threshold and superior electrical conductivity are attributed to the high aspect ratio, large specific surface area and uniform dispersion of the graphene nanosheets in PET matrix.



## 1. Introduction

Graphene, monolayer of carbon atoms arranged in a honeycomb network, has recently gained revolutionary aspirations [1–5] because of its remarkable electronic [4,6,7], thermal [8], and mechanical properties [9]. These unique properties make it a choice as inorganic fillers to improve electrical, thermal and mechanical properties of composite materials [5,10]. Several effective techniques have been developed for preparing graphene nanosheets, including chemical [5] and mechanical exfoliation [11], alkali metals intercalation and expansion [12], microwave chemical vapor deposition [13], substrate-based thermal decomposition [7], and thermal exfoliation of graphite oxide (GO) [14]. Among them, the thermal exfoliation and *in situ* reduction method can conveniently produce graphene nanosheets for mass production. More importantly, although insulating graphite oxide was converted to conducting graphene, the graphene nanosheets resulted through thermal exfoliation still contained some oxygen-containing groups [14], which will facilitate the dispersion of the nanosheets in polar polymers [10].

Graphene has exhibited its potential in improving electrical conductivity of polymers [15–17]. The polystyrene/graphene nanocomposites prepared by chemical modification and reduction in solution exhibited a percolation threshold as low as 0.1 vol.% [5], comparable to those observed in single-walled carbon nanotubes-based nanocomposites [18,19]. However, un-fully exfoliated graphite led to a much higher threshold (>0.6 vol.%) and a much lower electrical conductivity ($<10^{-2}$ S/m) even at high loading of 6.0 vol.% [20–22].

Compared to *in situ* exfoliation and solution mixing, melt compounding using commercial resins and conventional compounding devices such as extruder and mixer is more attractive because this approach provides manufacturers many degrees of freedom with regard to the selection of polymer grades and choice of graphene content. It is believed that melt compounding would be more economical and suitable for mass production than solution mixing. Actually, melt compounding has been successfully used to prepare conductive polymeric composites by using conducting fillers such as carbon nanotube (CNT) [23], carbon black and expanded graphite [24,25]. It has been confirmed that CNTs can substantially increase the electrical conductivity of PET nanocomposites with low filler loading, but it is expensive. As for cheap carbon black, higher loading is usually required to make a polymer electrically conductive. The low price and availability of pristine graphite in large quantities, coupled with the relative simple

* Corresponding author. Fax: +86 574 8668 5186.
** Corresponding author. Fax: +86 10 6442 8582.
*E-mail addresses:* wgzheng@nimte.ac.cn (W.-G. Zheng), yuzz@mail.buct.edu.cn (Z.-Z. Yu).

0032-3861/$ – see front matter © 2010 Elsevier Ltd. All rights reserved.
doi:10.1016/j.polymer.2010.01.027

fabrication process make graphene a potential choice as conductive fillers in the preparation of conductive PET nanocomposites. To the best of our knowledge, few papers have been published on PET/graphene nanocomposites prepared by conventional melt compounding. In this study, graphene nanosheets were prepared by complete oxidation of pristine graphite followed by thermal exfoliation and reduction. Subsequently, polyethylene terephthalate/graphene nanocomposites were fabricated by melt compounding. The microstructure of graphene, its dispersion in PET matrix, and the electrically conductive behavior of the resulting nanocomposites were studied.

## 2. Experimental

### 2.1. Materials

PET pellets were purchased and dried in vacuum oven at 150 °C for 5 h before use. Flaky pristine graphite with a mean size of 45 μm was bought from Qingdao Huatai Lubricant Sealing S&T (China). Graphene density is assumed as the theoretical graphite density of 2.28 g/cm$^3$ [18,26], and PET density is 1.34 g/cm$^3$ [27]. Fuming nitric acid (63%), sulfuric acid (98%), potassium chlorate (98%) and hydrochloric acid (37%) were obtained from Sinopharm Chemical Reagent (China).

### 2.2. Preparation of graphene

A technique, similar to that of McAllister and co-workers [14,28], was used to prepare bulk quantities of graphene nanosheets. Graphite oxide (GO) was prepared according to Staudenmaier method [14,29]. First of all, the reaction flask was purged with nitrogen and immersed in an ice bath, 40 g graphite was then added to the homogeneous mixture of concentrated nitric acid (270 ml) and sulfuric acid (525 ml) under vigorous stirring. After uniform dispersion of the graphite powder, 330 g potassium chlorate was added slowly to minimize the risk of explosion. The reaction was then allowed to last for 120 h at room temperature. After reaction, the slurry resultants were filtered and washed with excess deionized water and 5% HCl solution to remove the sulfuric ions ($SO_4^{2-}$), then GO aqueous solution was neutralized with potassium hydroxide solution. GO powder was extracted from the solution by using GQ75 high-speed centrifuge, and dried in an air-circulating oven at 135 °C for 24 h followed by another 24 h at 135 °C in a vacuum oven. As confirmed by McAllister and co-workers [28], 1050 °C was adequate for thermal exfoliation and *in situ* reduction of GO, this temperature was also adopted in the present work to thermally exfoliate GO. The dried GO powder was quickly inserted into a muffle furnace preheated to 1050 °C and held in the furnace for 30 s.

### 2.3. Fabrication of PET composites

PET/graphene nanocomposites were prepared by melt compounding at 285 °C using a Brabender mixer. Compounding was performed with an initial screw speed of 50 rpm/min for 4 min; then the screw speed was raised to 100 rpm/min within 1 min and the compounding was conducted at this speed for 5 min. The specimens for microscopy and electrical conductivity measurement were prepared by compression molding at 275 °C under a pressure of 15 MPa.

### 2.4. Characterization

The volume conductivity of moderately conductive composites (Conductance $>10^{-6}$ Sm) was measured with an Agilent 34401A digital multimeter and a YOKOGAWA 7651 voltage source by the two-probe method. For PET and composites with low conductivity (Conductance $\leq 10^{-6}$ Sm), the conductivity testing was performed using an EST121 ultrahigh resistance and micro current meter (Beijing EST Science & Technology CO. LTD) according to National Standard of China GB/1410-1989. A three-terminal fixture (two electrodes plus guard), similar to that proposed by the Standard ASTM D257 for volume conductance determination of flat specimens, was used for the measurement of low conductance. When measuring the volume resistivity, the test sample is placed between two electrodes and a potential difference is applied between them. The outer ring electrode connected to the guard was used to prevent surface leakage currents from being added into the measurement. Simultaneously, the circuit being measured was enclosed by a metal box to eliminate the electrostatic interference. Circular plates with 7 cm in diameter and 2.5 mm in thickness were fabricated for conductivity measurement. Sample surfaces were coated with silver paste to reduce contact resistance between sample and electrodes. For specimens with low conductivity, the side contacting with the unguarded electrode was wholly painted with silver paste, while for the other side only the parts contacting with the outer ring and inner guarded electrodes was covered. The resistance $R$ can be obtained directly from the multimeter, and thus the electrical conductivity $\sigma$ can be calculated from the geometry of the electrodes and the thickness of the sample by using Eq. (1)

$$\sigma = \frac{1}{\rho_v} = \frac{t}{RS} \tag{1}$$

where $\rho_v$ is volume resistivity, $t$ is sample thickness, and $S = [\pi(D_1 + \lambda)^2]/4$, $D_1$ is the diameter of inner electrode and $\lambda$ is the distance between inner and outer electrode. Three specimens of each sample were tested and the average value was reported as volume electrical conductivity.

The microstructures of graphene and its PET nanocomposites were characterized using a Tecnai G2 F20 TEM at an accelerating voltage of 100 kV. Graphene sheets were dispersed in methanol by ultrasonication and some pieces were collected on carbon-coated 300-mesh copper grids for observation. While for PET/graphene nanocomposites, the samples were embedded in epoxy resin, and cured at 80 °C for 6 h, and then ultrathin sections thinner than 100 nm were cryogenically cut with a diamond knife using a microtome and collected on 300-mesh copper grids. SEM observation of PET composites was performed using an FEI scanning electron microscope (Hitachi, S-4800) with an accelerating voltage of 5 kV. PET composites were freeze-fractured in liquid nitrogen and the fractured section was coated with a thin layer of platinum before observation.

The diffraction behavior of pristine graphite, GO and graphene was studied using a Bruker AXS X-ray diffractometer with CuKα radiation at a generator voltage of 40 kV and a generator current of 40 mA. The scans were carried out in the reflection mode at a scan rate of 10 °/min. Laser granularity analyzer (Malvern Zetasizer Nano ZS) was used to determine the lateral dimension of graphene in alcohol solution.

## 3. Results and discussion

### 3.1. Characterization of graphene

Fig. 1 shows the XRD spectra of pristine graphite, graphite oxide and graphene. The strong and sharp diffraction peak of pristine graphite at 26.6° completely disappeared after oxidization and instead a new peak at 13.9° appeared, indicating a complete oxidization of graphite [28,30], which is a prerequisite to obtain

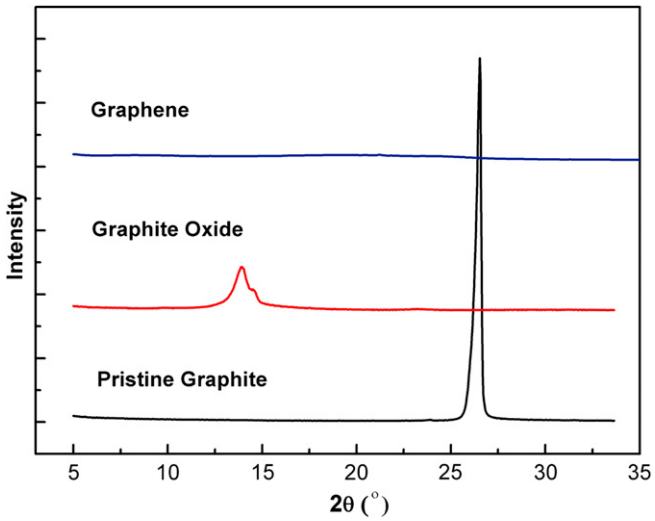


**Fig. 1.** X-ray diffraction patterns of pristine graphite, graphite oxide and graphene.

exfoliated graphene nanosheets by ultrasonication [5] or thermal expansion [14,28]. After thermal exfoliation of the completely oxidized graphite (GO), there was no apparent diffraction peak detected, which means the periodic structure of GO was eliminated and graphene nanosheets were formed. Fig. 2 shows TEM images of the graphene under low and high magnifications. Under low magnification, graphene looks like a transparent ultrathin film with a few thin ripples within the plane (Fig. 2a), quite different from the opaque and smooth feature of pristine graphite flakes. It is known that perfect two-dimensional graphene crystal was thermodynamically unstable [31], therefore, corrugations and ripples in the two dimension were formed for thermodynamic stability [32]. Thereby the transparency and rippled feature of graphene, in turn, suggests a fact that graphene sheets prepared in this study are wafer thin and consists of few-layer or even monolayer graphene. Furthermore, stacks of graphene sheets arranged with a roughly parallel structure can be clearly observed in the high-magnification TEM image from an edge-on view (Fig. 2b). The thickness of graphene sheets can thus be measured. Statistical results from many TEM images give an average thickness ~1.57 nm of the graphene sheets prepared in this study. In addition, the weak and diffuse selected area electron diffraction (SAED) pattern (the inset of Fig. 2b) also indicates the loss of long range ordering between graphene sheets and the ultrathin feature of the graphene [14]. However, it should be mentioned that the specific surface area of the graphene sheets measured with BET method is 555 $m^2/g$, much smaller than the theoretical value (2630 $m^2/g$) of single graphene sheet [33], indicating the existence of agglomerated and overlapped parts of the graphene sheets. In spite of this, a high aspect ratio (lateral dimension to thickness) of 146 for the graphene sheets is obtained based on the results from laser granularity analyzer. In contrast, pristine graphite flake has a lower aspect ratio (~36) and a smaller specific surface area (<10 $m^2/g$).

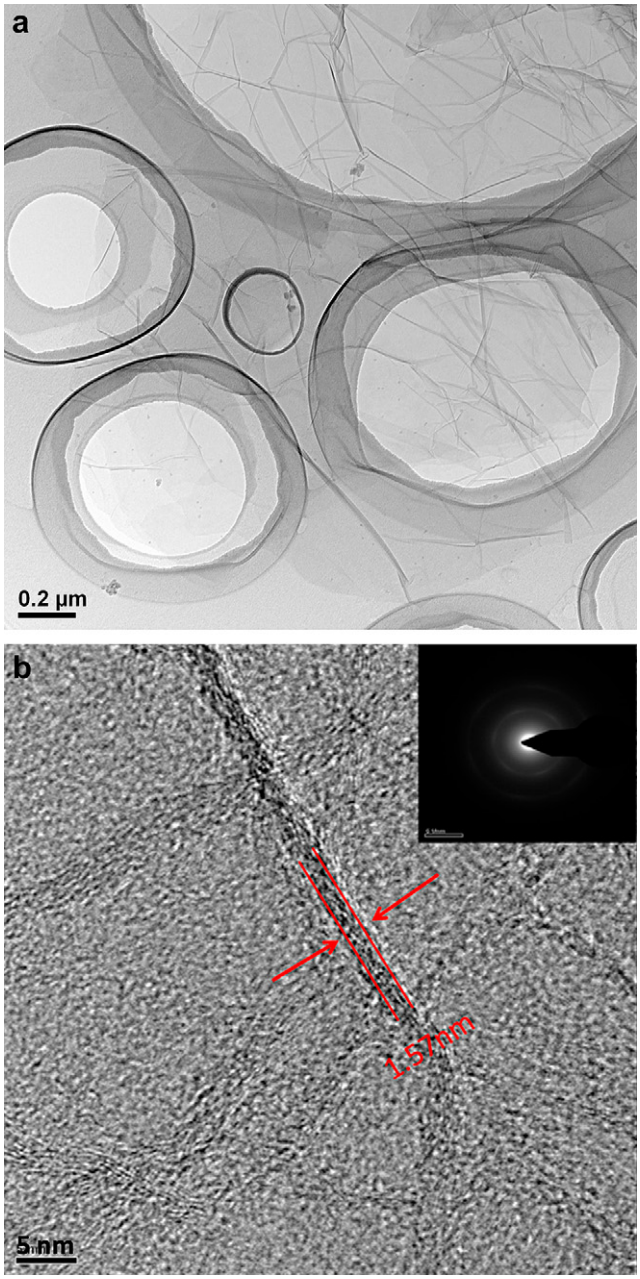


**Fig. 2.** TEM images of graphene under low (a) and high (b) magnifications. The scale bars are (a) 0.2 μm and (b) 5 nm. The inset is selected area electron diffraction (SAED) pattern of graphene.

### 3.2. Microstructure of PET/graphene nanocomposites

To clearly reveal the dispersion of graphene in PET matrix, Fig. 3 shows the microstructure of PET nanocomposite with 3 vol.% graphene. Graphene nanosheets were homogeneously dispersed in PET matrix and there are almost no large agglomerates observed (Fig. 3a). The good dispersion of graphene sheets should be due to the good interaction between the oxygen and hydroxyl functional groups on the surface of graphene and the polar groups of PET. In addition, a compact continuous network throughout the matrix is also observed (Fig. 3a). As proposed by Alig et al. [34], this conductive network can be considered as a network built by conductive fillers which are separated by local contact regions with polymer chains in-between. High magnification image (Fig. 3b) indicates that the network is composed of abundant thin stacks of a few sheets of monolayer graphene (black curly thin lines), which are bridged by the crumpled or overlapped graphene sheets (slightly thicker lines) (Fig. 3b). These wrinkled and overlapped graphene sheets can effectively link individual graphene sheets and carry high density of current, resulting in high electrical conductivity [35].

To demonstrate the strong interaction between the oxygen and hydroxyl functional groups on the surface of graphene and the

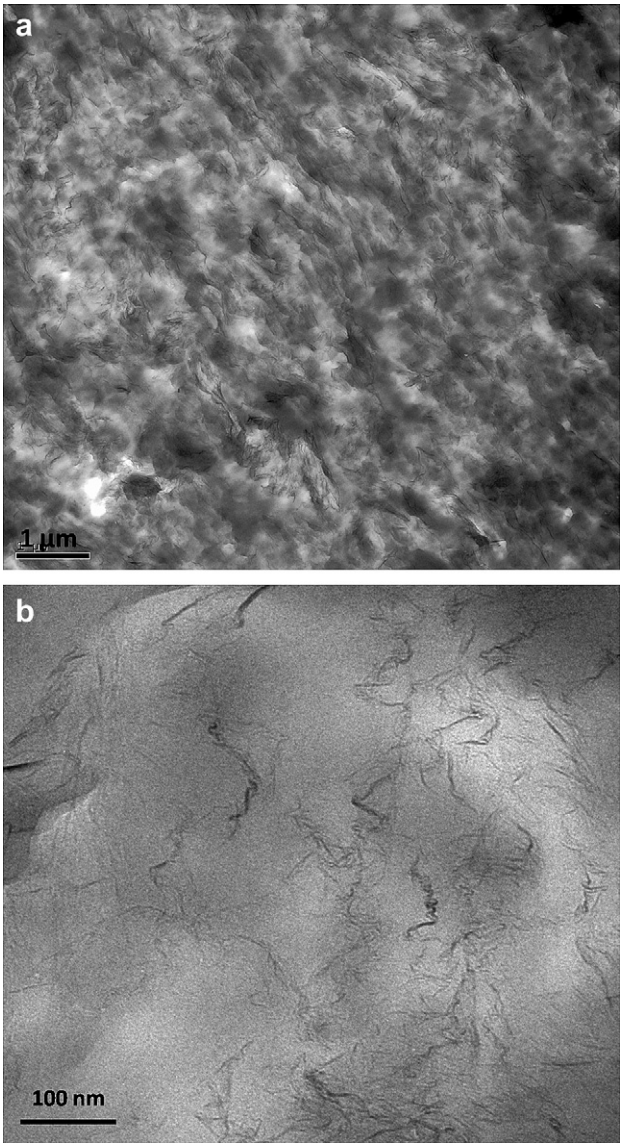


**Fig. 3.** Low (a) and high (b) magnification TEM micrographs of PET nanocomposite with 3 vol.% graphene. The scale bars are (a) 1 μm and (b) 100 nm.

polar groups of PET, Fig. 4 shows SEM image of cryo-fractured surface of PET nanocomposite with 1.2 vol.% graphene. It is seen that the graphene sheets were encapsulated by PET and the thickness of the sheets increased from 1.57 to ~50 nm (see the inset of Fig. 4). This confirms the strong interaction between graphene and PET. Due to the large specific surface area of the graphene nanosheets, the area of interface between graphene and PET is huge, providing numerous tunneling sites for electron transport [36,37].

### 3.3. Electrical properties of PET/graphene nanocomposites

Fig. 5 shows plots of electrical conductivity versus filler content for PET composites filled with graphene and pristine graphite. PET/graphene nanocomposites exhibit a sharp transition from insulator to semiconductor, and the inset of Fig. 5 indicates that their electrical conductivity ($\sigma$) obeys the power law [38]:

$$\sigma \propto \sigma_0(\varphi - \varphi_c)^{\upsilon} \quad (2)$$

where $\sigma_0$ is the bulk electrical conductivity of the fillers, $\varphi$ is the filler volume fraction, and $\upsilon$ is the critical exponent describing the

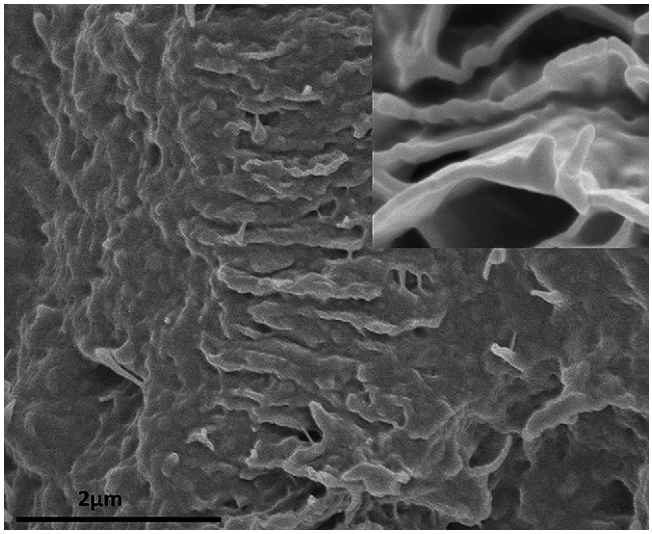


**Fig. 4.** SEM images of fractured surface of PET nanocomposite with 1.2 vol.% of graphene. The insert is a high-magnification SEM image of the same nanocomposite.

rapid variation of $\sigma$ near percolation threshold ($\varphi_c$). The percolation threshold is the critical content above which a continuous connected network is formed for the transport of electrons throughout the matrix. As shown in the inset of Fig. 5 for the double-logarithmic plot of electrical conductivity versus ($\varphi - \varphi_c$), the conductivity of PET/graphene nanocomposites agrees with the percolation behavior predicted by Eq. (2). Especially, when $\varphi_c = 0.47\%$ and $\upsilon = 4.22$, the straight line fits well with the experimental data.

For PET/graphene nanocomposites, the electrical conductivity quickly rises to $7.4 \times 10^{-2}$ S/m from $2.0 \times 10^{-13}$ with a slight increase in content from 0.47 to 1.2 vol.%. Actually, at 0.56 vol.% of the graphene content, the conductivity is $3.3 \times 10^{-5}$ S/m, which is higher than the antistatic criterion of $10^{-6}$ S/m. With only 3.0 vol.% graphene, the conductivity approaches to 2.11 S/m. On the contrary, PET/graphite composites show a higher percolation threshold of 2.4 vol.% and a broad percolation transition within a range of graphite content from 2.4 to 5.8 vol.%, the conductivity of PET/pristine graphite composite with 7.1 vol.% of graphite is only

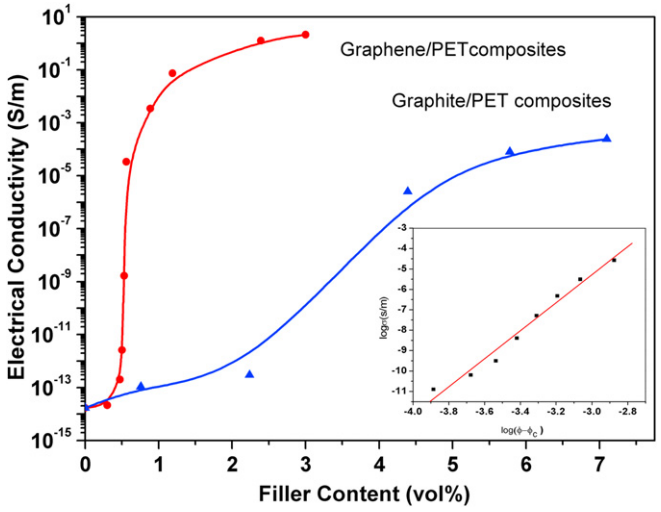


**Fig. 5.** Plots of electrical conductivity versus filler content for PET/graphene nanocomposites and PET/graphite composites. The inset is double-logarithmic plot of volume electrical conductivity versus ($\varphi - \varphi_c$).

$2.45 \times 10^{-4}$ S/m. These results indicate the advantage of graphene nanosheets.

To investigate the percolation behavior of graphene-filled nanocomposites, aspect ratio must be taken into consideration [15,36,39]. As revealed in Figs. 3 and 4, graphene nanosheets were evenly dispersed in matrix and covered with a thin layer of PET film, thus they can be assumed as isotropically distributed hard oblate spheroids of identical dimensions with soft shell in an insulating continuum host [40]. The shell thickness can be interpreted as a typical tunneling length between the particles, governing electrical connectivity of a composite. The percolation threshold, $p_c$, for infinite system can be obtained by extrapolating that for finite systems through the following scaling relations [41]:

$$\Delta(L) \propto L^{-1/\delta} \tag{3}$$

$$p_c^{\mathrm{eff}} - p_c \propto L^{-1/\delta} \tag{4}$$

where $\delta$ is the correlation length exponent, $\Delta$ represents the width of the percolation transition, $p_c^{\mathrm{eff}}$ is the effective percolation threshold for a system of linear size $L$. From thousands of simulations for variously sized lattices by Ambrosetti et al. [40], it is confirmed that the value of $\delta$ is around 0.9, and then $p_c$ can be consequently estimated from Eq. (4) by plotting $p_c^{\mathrm{eff}}$ against $L^{-\delta}$ for selected values of cell size $L$. As indicated by their simulation results, high aspect ratio entails a low percolation threshold. It is easy to understand that the higher aspect ratio of graphene than pristine graphite is consistent with the lower percolation threshold of PET/graphene nanocomposites.

Furthermore, if neglecting the limiting interaction distances to a shell of constant thickness from the presence of the hard core, namely, graphene and graphite are considered as permeable oblate particles, PET composite evolves to an idealized model consisting of completely permeable ellipsoids randomly dispersed in a matrix [42]. Here, $p_c$ can be directly predicted as $1.27\alpha/\beta$, where $\beta$ is the radius of revolution and $\alpha$ is the semiaxis length in the extreme oblate limit. Thus, $p_c$ can be easily calculated as 0.87 vol.% for PET/graphene nanocomposites and 3.34 vol.% for PET/graphite composites. These values are higher than those obtained experimentally from curves of Fig. 5. This difference between $p_c$ and $\varphi_c$ may be, in part, due to the assumption that graphite and graphene were permeable, and in part, to the fact that Eq. (2) did not consider tunneling mechanism. The permeable assumption allows regions of space to be occupied by parts of more than one sheet and thereby the critical volume of fillers is overestimated. In addition, the unfavorable geometries of oblate particles also tend to reduce the interparticle connectivity and increase the percolation point [43]. It is now believed that physically contacted network is adequate but not absolutely necessary for current flow in insulator–conductor composites, since electrons can transmit between isolated particles by tunneling through thin polymer layer in-between [37,44–46].

It is worthwhile to mention that the efficiency of graphene in improving conductivity of PET is comparable to or even better than that of CNTs. Hu et al. [47] reported a low electrical percolation threshold (0.9 wt.%) in PET/MWCNT nanocomposites fabricated via coagulation, and the electrical conductivity reached $10^{-2}$ S/m at higher filler loading ($\sim$5 wt.%). An even lower percolation threshold was reported by Steinert and Dean [37] in PET/SWCNT nanocomposite films prepared using a solution mixing and casting method. It was shown that sufficient conductivity for antistatic and electrostatic dissipation purpose was achieved at 0.5 wt.% SWCNT [37], which was reasonable. On one hand, solution casting of a film is very efficient in forming a conductive network due to the 2-dimentional distribution of CNT; on the other hand, the aspect ratio of CNT could be retained due to the less serious damage of CNT during the solution mixing. Compared to solution mixing, melt compounding like extrusion would inevitably shorten CNT and graphene and thus reduce their aspect ratios, which is not beneficial for achieving low percolation threshold and high conductivity [48–50]. Mild condition of melt compounding is required to retain the aspect ratio of graphene sheets. The low percolation threshold obtained in the current study should be attributed to the high aspect ratio, large specific surface area and the good dispersion of graphene in PET matrix.

## 4. Conclusions

Graphene sheets were prepared by chemical oxidation of pristine graphite flakes followed by thermal exfoliation and reduction of graphite oxide. PET/graphene nanocomposites prepared by melt compounding exhibit superior electrical conductivity with a low percolation threshold of 0.47 vol.%. A high electrical conductivity of 2.11 S/m of PET nanocomposite was achieved with only 3.0 vol.% of graphene, which is even adequate for EMI shielding. The low percolation threshold and superior electrical conductivity are attributed to the high aspect ratio, large specific surface area and uniform dispersion of the graphene nanosheets in PET matrix.

## References


[1] Novoselov KS, Geim AK, Morozov SV, Jiang D, Katsnelson MI, Grigorieva IV, et al. Nature 2005;438(7065):197–200.
[2] Novoselov KS, Jiang Z, Zhang Y, Morozov SV, Stormer HL, Zeitler U, et al. Science 2007;315(5817):1379.
[3] Heersche HB, Jarillo-Herrero P, Oostinga JB, Vandersypen LMK, Morpurgo AF. Nature 2007;446(7131):56–9.
[4] Zhang YB, Tan YW, Stormer HL, Kim P. Nature 2005;438(7065):201–4.
[5] Stankovich S, Dikin DA, Dommett GHB, Kohlhaas KM, Zimney EJ, Stach EA, et al. Nature 2006;442(7100):282–6.
[6] Zhang YB, Small JP, Amori MES, Kim P. Phys Rev Lett 2005;94(17):176803.
[7] Berger C, Song ZM, Li TB, Li XB, Ogbazghi AY, Feng R, et al. J Phys Chem B 2004;108(52):19912–6.
[8] Balandin AA, Ghosh S, Bao WZ, Calizo I, Teweldebrhan D, Miao F, et al. Nano Lett 2008;8(3):902–7.
[9] Lee C, Wei XD, Kysar JW, Hone J. Science 2008;321(5887):385–8.
[10] Ramanathan T, Abdala AA, Stankovich S, Dikin DA, Herrera-Alonso M, Piner RD, et al. Nat Nanotechnol 2008;3(6):327–31.
[11] Novoselov KS, Geim AK, Morozov SV, Jiang D, Zhang Y, Dubonos SV, et al. Science 2004;306(5696):666–9.
[12] Viculis LM, Mack JJ, Kaner RB. Science 2003;299(5611):1361.
[13] Wang XB, You HJ, Liu FM, Li MJ, Wan L, Li SQ, et al. Chem Vapor Depos 2009;15(1–3):53–6.
[14] McAllister MJ, Li JL, Adamson DH, Schniepp HC, Abdala AA, Liu J, et al. Chem Mater 2007;19(18):4396–404.
[15] Xie SH, Liu YY, Li JY. Appl Phys Lett 2008;92(24):243121.
[16] Kim H, Macosko CW. Macromolecules 2008;41(9):3317–27.
[17] Liang JJ, Wang Y, Huang Y, Ma YF, Liu ZF, Cai FM, et al. Carbon 2009;47(3):922–5.
[18] Grossiord N, Loos J, Koning CE. J Mater Chem 2005;15(24):2349–52.
[19] McLachlan DS, Chiteme C, Park C, Wise KE, Lowther SE, Lillehei PT, et al. J Polym Sci Pol Phys 2005;43(22):3273–87.
[20] Kalaitzidou K, Fukushima H, Drzal LT. Carbon 2007;45(7):1446–52.
[21] Weng WG, Chen GH, Wu DJ. Polymer 2005;46(16):6250–7.
[22] Zheng WG, Wong SC, Sue HJ. Polymer 2002;43(25):6767–73.
[23] Li ZF, Luo GH, Wei F, Huang Y. Compos Sci Technol 2006;66(7–8):1022–9.
[24] Lagreve C, Feller JF, Linossier I, Levesque G. Polym Eng Sci 2001;41(7):1124–32.
[25] Zhang M, Li DJ, Wu DF, Yan CH, Lu P, Qiu GM. J Appl Polym Sci 2008;108(3):1482–9.
[26] Kelly B. Physics of graphite. London Englewood N.J: Applied Science Publishers; 1981. pp. 267–361.
[27] Cobbs WH, Burton RL. J Polym Sci 1953;10(3):275–90.
[28] Schniepp HC, Li JL, McAllister MJ, Sai H, Herrera-Alonso M, Adamson DH, et al. J Phys Chem B 2006;110(17):8535–9.
[29] Staudenmaier L. Ber Dtsch Chem Ges 1898;31:1481–99.
[30] Wang GX, Yang J, Park J, Gou XL, Wang B, Liu H, et al. J Phys Chem C 2008;112(22):8192–5.
[31] Meyer JC, Geim AK, Katsnelson MI, Novoselov KS, Booth TJ, Roth S. Nature 2007;446(7131):60–3.
[32] Carlsson JM. Nat Mater 2007;6(11):801–2.
[33] Peigney A, Laurent C, Flahaut E, Bacsa RR, Rousset A. Carbon 2001;39(4):507–14.
[34] Alig I, Lellinger D, Dudkin SM, Potschke P. Polymer 2007;48(4):1020–9.
[35] Halperin BI, Feng S, Sen PN. Phys Rev Lett 1985;54(22):2391–4.

[36] Yao SH, Dang ZM, Jiang MJ, Xu HP. Appl Phys Lett 2007;91(21):212901.
[37] Steinert BW, Dean DR. Polymer 2009;50(3):898–904.
[38] Stauffer D. An introduction to percolation theory. London and Philadelphia: Taylor and Fansis; 1985. pp. 325–55.
[39] Ma HM, Gao XL. Polymer 2008;49(19):4230–8.
[40] Ambrosetti G, Johner N, Grimaldi C, Danani A, Ryser P. Phys Rev E 2008;78(6):061126.
[41] Rintoul MD, Torquato SJ. Phys A: Math Gen 1997;30(16):585–92.
[42] Garboczi EJ, Snyder KA, Douglas JF, Thorpe MF. Phys Rev E 1995;52(1):819–28.
[43] Yi YB, Tawerghi E. Phys Rev E 2009;79(4):041134.
[44] Balberg I. Phys Rev Lett 1987;59(12):1305–8.
[45] Quivy A, Deltour R, Jansen AGM, Wyder P. Phys Rev B 1989;39(2):1026–30.
[46] Toker D, Azulay D, Shimoni N, Balberg I, Millo O. Phys Rev B 2003;68(4):041403.
[47] Hu GJ, Zhao CG, Zhang SM, Yang MS, Wang ZG. Polymer 2006;47(1):480–8.
[48] Dasari A, Yu ZZ, Mai YW. Polymer 2009;50(16):4112–21.
[49] Xiao P, Xiao M, Gong KC. Polymer 2001;42(11):4813–6.
[50] Zheng W, Wong SC. Compos Sci Technol 2003;63(2):225–35.